Anatase Mesoporous TiO$_2$ Nanofibers with High Surface Area for Solid-State Dye-Sensitized Solar Cells

Wei Zhang, Rui Zhu, Lin Ke, Xizhe Liu, Bin Liu,* and Seeram Ramakrishna*

Mesoporous nanofibers (NFs) with a high surface area of 112 m^2/g have been prepared by electrospinning technique. The structures of mesoporous NFs and regular NFs are characterized and compared through scanning electron microscope (SEM), transmission electron microscopy (TEM), X-ray diffraction (XRD) and selected area electron diffraction (SAED) studies. Using mesoporous TiO$_2$ NFs as the photoelectrode, solid-state dye-sensitized solar cells (SDSCs) have been fabricated employing D131 as the sensitizer and P3HT as the hole transporting material to yield an energy conversion efficiency (η) of 1.82%. A J_{sc} of 3.979 mA cm^{-2} is obtained for mesoporous NF-based devices, which is 3-fold higher than that (0.973 mA cm^{-2}) for regular NF-based devices fabricated under the same condition ($\eta = 0.42\%$). Incident photon-to-current conversion efficiency (IPCE) and dye-desorption test demonstrate that the increase in J_{sc} is mainly due to greatly improved dye adsorption for mesoporous NFs as compared to that for regular NFs. In addition, intensity modulated photocurrent spectroscopy (IMPS) and intensity modulated photovoltage spectroscopy (IMVS) measurements indicate that the mesopores on NF surface have very minor effects on charge transport and collection. Initial aging test proves good stability of the fabricated devices, which indicates the promise of mesoporous NFs as photoelectrode for low-cost SDSCs.

1. Introduction

Solid-state dye-sensitized solar cells (SDSCs) which incorporate nanocrystalline TiO$_2$ films and organic hole transport materials (HTMs) have aroused great scientific interests because they intrinsically avoid the leakage problem of conventional liquid-electrolyte dye-sensitized solar cells (LDSCs).[1] In addition, SDSCs combine the advantages of inorganic semiconductors such as mechanical and chemical stability with the unique properties of organic HTM such as easy film formation and adjustable functionality by molecular design.[2] Over the past decade, significant progress has been made for SDSCs and the highest efficiency of ~5% is achieved based on devices with organic small molecule 2,2′,7,7′-tetrakis-(N,N-di-4-methoxyphenylamino)-9,9′-spiro-bifluorene (spiro-OMeTAD) as the HTM.[3]

Despite of the potential advantages of SDSCs, their device efficiencies are still far behind the "champion cell" utilizing liquid electrolyte.[4] One major factor is insufficient light harvesting caused by limited TiO$_2$ film thickness.[3,5] To increase light absorption of thin TiO$_2$ films, several strategies have proven to be effective. One is to increase the molar extinction coefficient of dye molecules. In this context, organic dyes are more attractive than ruthenium dyes due to their high extinction coefficient, tunable energy levels and low cost. Several organic dye-based SDSCs have shown improved performance as compared to those based on ruthenium dyes.[6–8] Another

Mr. W. Zhang, Dr. R. Zhu, Dr. X. Liu, Prof. B. Liu
Department of Chemical and Biomolecular Engineering
National University of Singapore
Singapore 117576, Singapore
E-mail: cheliub@nus.edu.sg

Prof. S. Ramakrishna
Nanoscience and Nanotechnology Initiative
National University of Singapore
Singapore 117576, Singapore
E-mail: seeram@nus.edu.sg

Dr. L. Ke
Institute of Materials Research and Engineering
3 Research Link, Singapore 117602, Singapore

strategy is to improve dye loading by increasing the surface area of thin TiO$_2$ films. One example is to replace TiO$_2$ films composed of randomly oriented nanoparticles with organized mesoporous TiO$_2$ structures.[9] In addition, light absorption in devices could be further enhanced by increasing reflectivity of the counter electrodes.[3] Another important factor that restricts SDSC performance is the slow charge transport in randomly oriented TiO$_2$ nanoparticle film, which limits charge collection efficiency.[10,11] Consequently, many studies focused on replacing TiO$_2$ nanoparticle film with one-dimensional (1 D) nanostructures, such as TiO$_2$ nanowires, nanorods and nanotubes to provide a direct conduction pathway for rapid collection of photoelectrons.[12–14] Such a strategy has been proven successful for LDSCs, but is rarely applied for SDSCs based on TiO$_2$ photoelectrode and organic HTM. This could be due to the small surface area of 1 D nanostructured photoelectrodes that further limits light harvesting in thin TiO$_2$ films for SDSCs. Traditional methods to increase the surface area of 1 D nanostructured photoelectrodes of LDSCs, *e.g.,* by mixing TiO$_2$ nanowires or nanorods with TiO$_2$ nanoparticles,[15,16] are not suitable for SDSCs because the introduction of TiO$_2$ nanoparticles will decrease the film porosity, which affects the pore filling of TiO$_2$ film with organic HTM. As a consequence, to increase the surface area of 1 D nanostructured TiO$_2$ film without compromising the penetration of organic HTM is the bottleneck for further improving device performance. Up to date, great efforts toward improving the penetration of organic HTM have been made by Grimes,[17,18] Darling[19] and McGehee's groups.[20] Recently, a significant progress was reported by Grimes and coworkers, who developed a highly efficient heterojunction solar cell based on TiO$_2$ nanotube arrays modified with organic dye and poly(3-hexylthiophene) (P3HT) as HTM.[21]

In this contribution, we report the fabrication of SDSCs based on mesoporous TiO$_2$ nanofiber (mesoporous NF) photoelectrodes and P3HT as HTM. The motivation for such design is based on the following considerations. Firstly, mesoporous TiO$_2$ nanofibers provide a large surface area for dye adsorption which could improve light harvesting in thin TiO$_2$ films. Secondly, numerous literatures have proven that 1 D nanostructure could facilitate charge collection in TiO$_2$ photoelectrodes.[12–14] Thirdly, the micron-size pores formed between TiO$_2$ nanofibers could be beneficial for the penetration of organic HTM. For comparison, TiO$_2$ nanofibers with smooth surfaces (regular NFs) are also used for SDSCs. The device efficiency of SDSCs based on mesoporous NFs was greatly improved as compared to that based on regular NFs.

2. Results and Discussion

The mesoporous NFs were prepared by electrospinning technique using Ti(OEt)$_4$ as the inorganic precursor and amphiphilic triblock copolymer F127 as the structure directing agent. The formation of mesopores on nanofiber surface is due to solvent evaporation-induced self-assembly of inorganic precursor.[22] Briefly, the initial concentration of F127 (c$_0$) in the inorganic precursor solution is lower than its critical micelle concentration (cmc). During electrospinning,
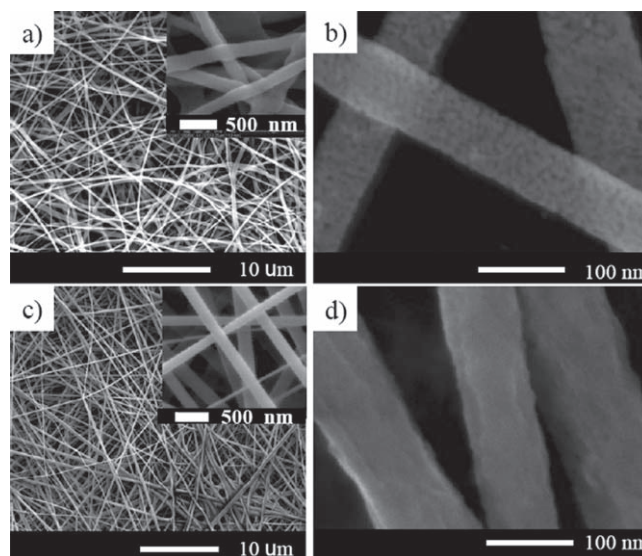

Figure 1. SEM images of mesoporous NFs (as-spun (a) and calcined (b)) and regular NFs (as-spun (c) and calcined (d)). Insets of Figures (a) and (c) show the enlarged SEM images of as-spun NFs.

the progressive evaporation of 1-butanol concentrates the surfactant to a concentration that is higher than its cmc, which drives the self-assembly of inorganic precursor and surfactant micelle to form mesophases.[22] The morphologies of electrospun mesoporous and regular NFs before and after calcination were characterized by scanning electron microscope (SEM) and the results are shown in **Figure 1**. Before calcination, the as-spun nanofibers (Figure 1a and 1c) are quite continuous and each nanofiber keeps the cross-section uniformity throughout the length direction, indicating good control of the electrospinning conditions. As shown in the insets of Figure 1a and 1c, the average diameters of as-spun mesoporous and regular NFs are 205 ± 20 nm and 220 ± 30 nm, respectively. After calcination at 450 °C in air for 1 h, the mesopores with an average pore size of 6 ± 0.5 nm are clearly observed on the mesoporous NF surfaces (Figure 1b). In addition, each individual nanofiber has an average diameter of 96 ± 14 nm with cross-sectional uniformity. By contrast, the regular NFs have smooth surfaces (Figure 1d) with an average diameter of 104 ± 15 nm. As compared to the as-spun nanofibers, the diameters of calcined nanofibers decreased obviously. Such phenomenon is universal in preparing electrospun TiO$_2$ nanofibers and has been observed by several research groups.[23–27] The reduction of TiO$_2$ nanofiber diameter after calcination is due to the loss of polymer binder (F127 or PEO) from the as-spun nanofibers and the crystallization of titania.[23–25]

The morphologies of mesoporous and regular NFs after calcination were further studied by transmission electron microscopy (TEM). **Figure 2**a shows the TEM image of a single mesoporous NF. The nanofiber is composed of uniformly dispersed but loosely compacted TiO$_2$ grains with an average grain size of 9.3 ± 1.9 nm. Voids exist between adjacent grains to form worm-like patterns on the nanofiber surface, which indicate that the mesoporous NF exhibits
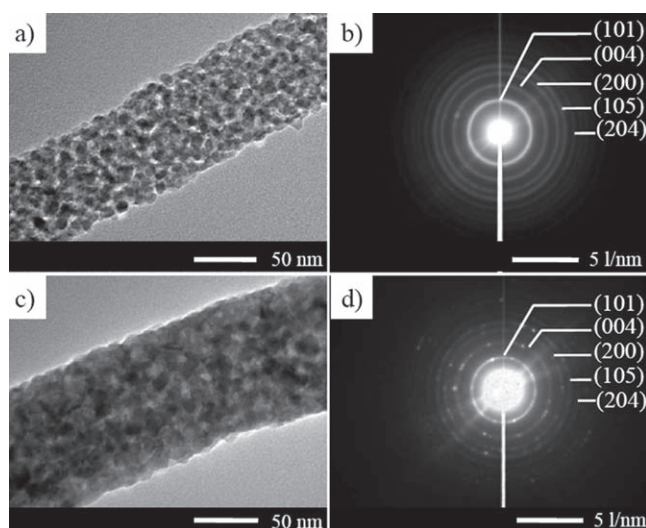
Figure 2. TEM images of calcined mesoporous (a) and regular (c) NFs. The corresponding SAED patterns are shown in (b) and (d) for mesoporous and regular NFs, respectively.
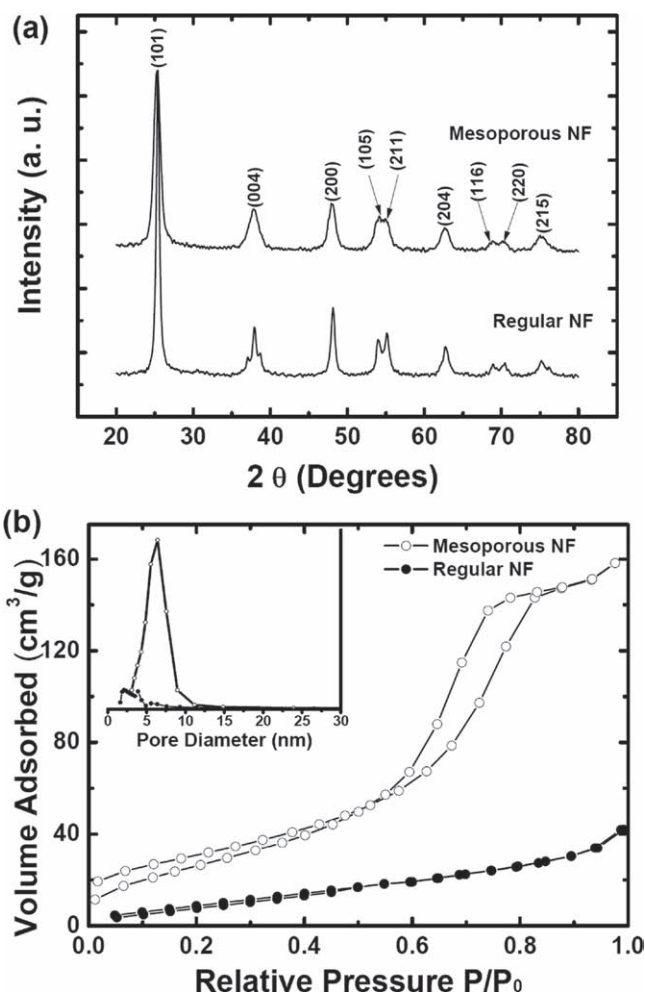

Figure 3. (a) XRD patterns of mesoporous and regular NFs (b) N_2 adsorption-desorption isotherm and the pore size distribution (inset) of mesoporous and regular NF films.

less ordered 3D mesostructures.[28] For regular NF, the TiO_2 grains (18.3 ± 3.4 nm) are closely packed without obvious voids (Figure 2c), which correlate well with the SEM image. Figure 2b and 2d show the corresponding selected area electron diffraction (SAED) patterns of calcined mesoporous and regular NFs, respectively. All the polycrystalline diffraction rings are indexed to the anatase phase of TiO_2, and there is no secondary phase or impurities detected.

The crystal structures of calcined mesoporous and regular NFs were investigated by X-ray diffraction (XRD) analysis (**Figure 3**a). All the peaks are indexed to the anatase phase of TiO_2, which correlate well with the results from SAED analysis. From the Scherrer equation[29] and the anatase (101) peak at $2\theta = 25.3°$, the grain size of TiO_2 is calculated to be 8.6 and 17.5 nm for mesoporous and regular NFs, respectively. These results are in agreement with those shown in Figure 2a and 2c.

Figure 3b shows the N_2 adsorption-desorption isotherms of the mesoporous and regular NF films, which were prepared by spin-coating the corresponding NF paste on FTO substrate followed by calcination at 450 °C for 30 min. A type-IV isotherm with a large hysteresis loop between the H1- and H2-types is obtained for mesoporous NF film, indicating the presence of well-defined mesopores on nanofiber surfaces.[30–32] However, a type II-like isotherm is obtained for the regular NF film, which demonstrates that no typical mesopores exist on the nanofiber surface. The pore size distribution was calculated based on BJH (Barrett-Joyner-Halenda) method and the desorption branch of the isotherm. A narrow pore-size distribution is observed for mesoporous NFs with an average pore size of 6.4 nm, which is in accordance with the size observed by SEM. By contrast, regular NFs show multi-modal pore-size distribution. From BET analysis, the surface area of the mesoporous NF film is 112 m²/g, which is ~2 times higher than that of the regular NF film (40 m²/g). The total pore volumes for the mesoporous and regular NF films are 0.272 cm³/g and 0.0649 cm³/g, respectively. In addition,

the porosity (P)[33] values of the regular and mesoporous NF films are calculated to be 20.2% and 51.4%, respectively. These results demonstrate that the mesoporous nanostructure increases the surface area and improves the porosity of 1 D nanostructured TiO_2 film significantly as compared to that for the regular NF film.

To evaluate the potential of mesoporous NFs as photoelectrode, SDSCs were fabricated by spin-coating a P3HT layer on the top of a D131-anchored TiO_2 NF layer. The device configuration is shown in **Figure 4**a, and the chemical structure of D131 is shown in Figure 4b. The devices based on regular NF photoelectrode were fabricated under the same conditions. Detailed device fabrication procedures are described in the experimental section. The TiO_2 film thickness was kept at 1.8 μm and the active cell area was 0.10 cm². Figure 4c displays the energy band diagram for each component in the device. The detailed determination of the energy levels for D131 and P3HT is shown in the Supporting Information (Figure S1–S3). The lowest unoccupied molecular orbital (LUMO) level of D131 (–2.90 eV) is well above the conduction band edge of TiO_2 (~–4.00 eV vs vacuum level).[34] Therefore, electron injection from the LUMO of D131 into the conduction band
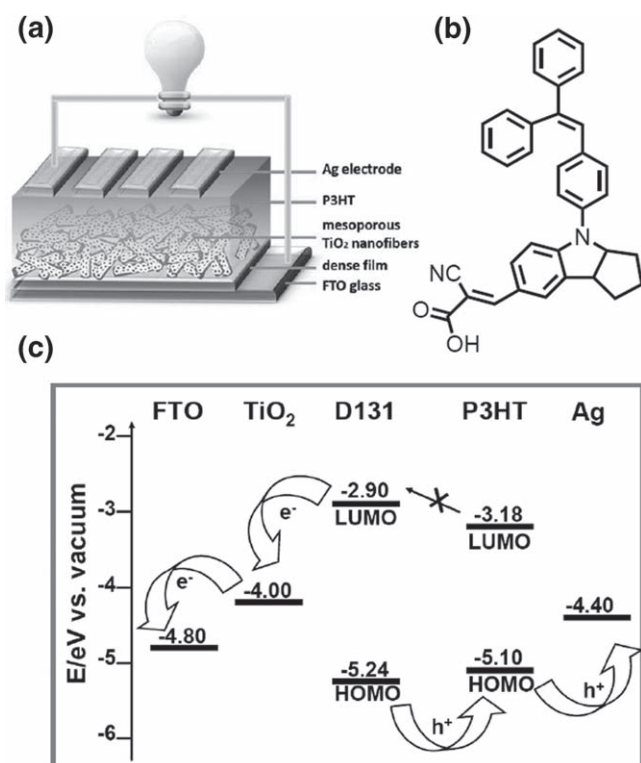
Figure 4. (a) The configuration of a typical device employing mesoporous TiO₂ nanofibers as the photoelectrode, D131 as the sensitizer and P3HT as the hole transporting material. (b) The chemical structure of D131. (c) Energy band diagram of each component in the device.
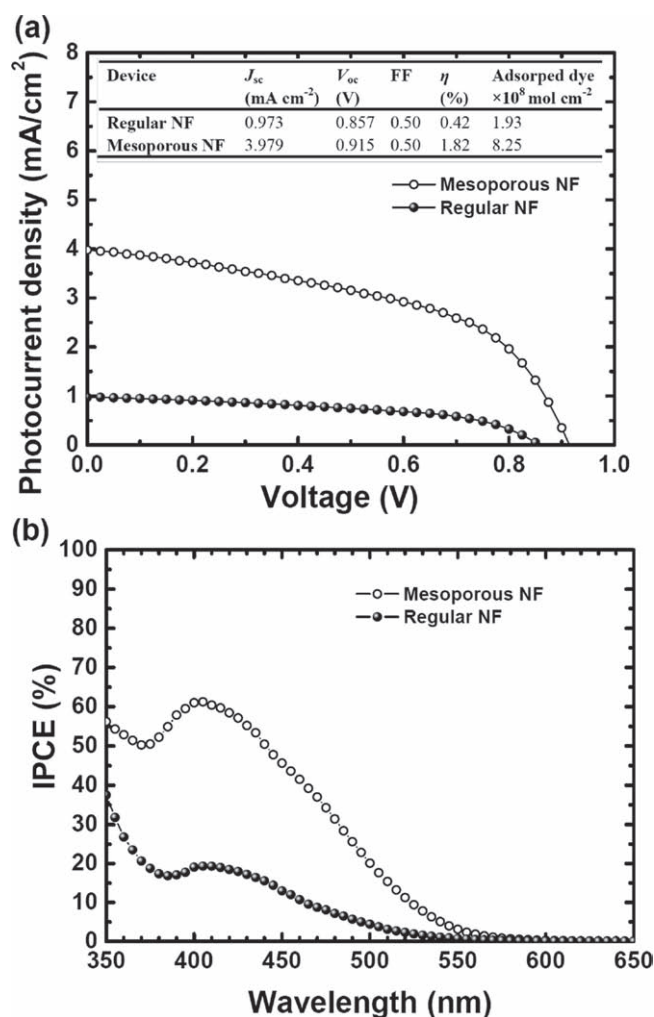

Figure 5. Typical photocurrent density-voltage curves (a) and IPCE spectra (b) of SDSCs based on mesoporous and regular NF photoelectrodes.

of TiO₂ is energetically feasible. Meanwhile, the highest occupied molecular orbital (HOMO) of D131 (−5.24 eV) is lower than that of P3HT (−5.10 eV), ensuring the hole conduction from D131 to P3HT. However, the electron transfer pathway from the LUMO of P3HT to the conduction band of TiO₂ should be blocked by D131, as the LUMO level of D131 is ~ 0.30 eV higher than that of P3HT (−3.18 eV). This energy band diagram indicates that the function of P3HT in the present SDSC is largely HTM, even though it can absorb a fraction of incident light that passes through the D131-sensitized TiO₂ film.

Figure 5a shows the typical photocurrent density-voltage curves obtained under irradiation of 100 mW cm⁻². All data are repeated in three independent devices. For devices based on regular NFs, a short-circuit current density (J_{sc}) of 0.973 mA cm⁻², an open-circuit voltage (V_{oc}) of 0.857 V and a fill factor (FF) of 0.50 were achieved, resulting in an energy conversion efficiency (η) of 0.42%. The device performance was greatly improved for mesoporous NF-based devices, which gave J_{sc} of 3.979 mA cm⁻², V_{oc} of 0.915 V, FF of 0.50 and η of 1.82%. The improved energy conversion efficiency is thus mainly attributed to ~ 3-fold increase in J_{sc} as compared to that for regular NF-based devices. To understand the difference in J_{sc}, dye-desorption experiment was first performed. As shown in the last column of the inset of Figure 5a, the dye loading for mesoporous NF film is 8.25×10^{-8} mol cm⁻², which is ~ 3.3-fold more relative to that for regular NF film (1.93×10^{-8} mol cm⁻²). The improved J_{sc} value for mesoporous NF-based devices is further verified by the incident photon-to-current

conversion efficiency (IPCE) spectra, as shown in Figure 5b. The maximum IPCE values obtained at 410 nm are 61% and 19% for the mesoporous and regular NF-based devices, respectively, suggesting that light harvesting is significantly improved for mesoporous NF-based devices as compared to that for regular NFs.

To obtain deep insights into the effect of different NF structures on device performance, intensity modulated photocurrent spectroscopy (IMPS) and intensity modulated photovoltage spectroscopy (IMVS) have also been employed to investigate the charge transport and recombination characteristics in mesoporous and regular NF-based devices. In these measurements, frequency-dependent photocurrent or photovoltage responses of a typical device to modulated incident light were recorded. From the IMPS measurements (**Figure 6**a), the transport time (τ_d) of injected electrons through TiO₂ film can be calculated from the equation $\tau_d = 1/(2\pi f_{d,\,min})$,[35] where $f_{d,\,min}$ is the characteristic frequency at the minimum of the IMPS imaginary component. Thus, τ_d values are estimated to be 1.05 and 0.88 ms in mesoporous and regular NF films, respectively. In addition, from the equation $D_n = d^2/(2.35\tau_d)$,[36] where d is the thickness of the photoelectrode
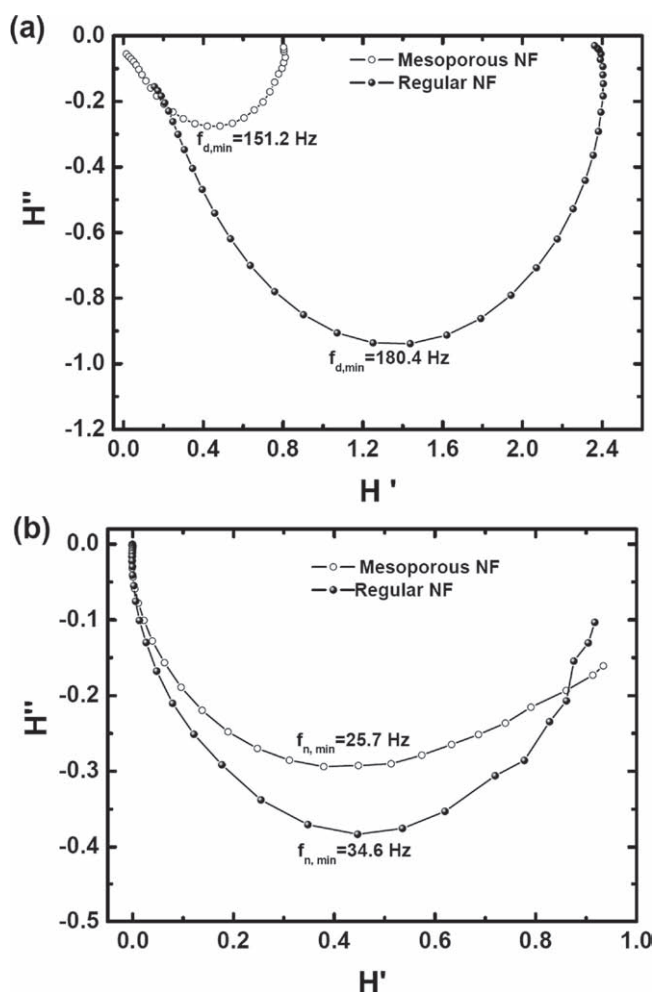
Figure 6. IMPS (a) and IMVS (b) of SDSCs based on mesoporous and regular NF photoelectrodes.

(~1.8 µm), the electron diffusion coefficients (D_n) in mesoporous and regular NF films are calculated to be 1.31×10^{-5} and 1.57×10^{-5} cm²s⁻¹, respectively. Although the mesoporous NF film has a much higher pore volume (0.272 cm³/g) as compared to that for regular NF film (0.0649 cm³/g), which could result in a more tortuous propagation of electrons and a more frequent electron trapping and detrapping events in TiO_2 layer,[37,38] the only slightly smaller D_n for mesoporous NF films indicates that the retardation of electron transportation caused by mesopores is not very serious in this case. This could be probably due to the $TiCl_4$ post-treatment step in device fabrication, which partially fills the pores in mesoporous NFs and to some extent offsets the original difference in NF structures. A similar phenomenon has also been observed by Kim *et al.*[39]

From the IMVS measurements (Figure 6b), the recombination lifetime (τ_n) was calculated using the equation $\tau_n = 1/(2\pi f_{n,min})$,[35] where $f_{n,min}$ is the characteristic frequency at the minimum of the IMVS imaginary component. Thus, τ_n values are estimated to be 6.20 and 4.60 ms for mesoporous and regular NF films, respectively. In general, the longer lifetime indicates a slower recombination rate between photoelectrons in the conduction band of TiO_2 and the hole

conductor P3HT. This result is consistent with the improved V_{oc} for mesoporous NF-based devices (0.915 V) as compared to that for regular NF-based devices (0.857 V).[14] Furthermore, the charge collection efficiency, η_{cc}, described by the equation $\eta_{cc} = 1-\tau_d/\tau_n$,[40] is calculated to be 83.0% and 80.8% for mesoporous and regular NF films, respectively. Considering the obtained dye-desorption and IPCE results, the similar charge collection efficiency for mesoporous and regular NF films further confirms that the significant difference in device photocurrent is mainly due to different dye adsorption in these two TiO_2 NF films.

To evaluate the long-term device stability, a typical device stored in a glove-box for ~6 months was retested, which gave J_{sc} of 3.887 mA cm⁻², V_{oc} of 0.918 V, FF of 0.48 and η of 1.73%. As compared to the typical performance of a freshly prepared cell (Figure 5a), the aged cell sustained ~94% of its initial device efficiency, demonstrating good stability of the fabricated devices. Future aging test should be performed under more stringent conditions (AM 1.5 full sunlight soaking for 1000 h at 60 °C), which needs special sealing technique for SDSCs as the exposure of P3HT to the extrinsic oxygen or water will affect the intrinsic device-stability.[41,42]

3. Conclusions

In summary, we prepared two types of TiO_2 nanofibers in pure anatase phase by electrospinning technique. One is regular NFs with smooth surfaces, and the other is mesoporous NFs with uniform pore size distribution. A high BET surface area of 112 m²/g was obtained for mesoporous NF films due to the existence of mesopores on the nanofiber surface. Solid-state dye-sensitized solar cells were fabricated based on these nanofibers using organic indoline dye D131 as the sensitizer and P3HT as the hole transporting material. As compared to the low J_{sc} (0.973 mA cm⁻²) and η (0.42%) for regular NF-based devices, a three-fold increase in J_{sc} (3.979 mA cm⁻²) was obtained for mesoporous NF-based devices, yielding an energy conversion efficiency of 1.82%. The increase in J_{sc} was mainly attributed to the greatly improved dye adsorption for mesoporous NFs. In addition, IMPS and IMVS analysis reveals that the mesopores on NF surfaces have very minor effects on charge transport and collection relative to that for regular NFs. The initial aging test proved good stability of the devices. Considering the simple and cost-effective features of electrospinning technique, the mesoporous TiO_2 nanofibers synthesized in this work are promising to serve as photoelectrode for low-cost SDSCs.

4. Experimental Section

Preparation of mesoporous and regular NFs by electrospinning: The precursor gel for electrospinning of mesoporous NFs was prepared by slow addition of 1.0 mL of acetic acid into 1.0 mL of titanium ethoxide (Ti(OEt)₄, Aldrich) under vigorous stirring. Separately, 0.5 g block copolymer F127 (H(C₂H₅O)₁₀₆(C₃H₇O)₇₀(C₂H₅O)₁₀₆OH, BASF) dissolved in 2.5 mL of 1-butanol (Aldrich) was added into the acetic acid/Ti(OEt)₄ solution. This final mixture was

aged at ambient temperature for 3 h to give a spinnable sol.[9] For comparison, regular NFs were electrospun from the precursor gel consisting of 0.45 g poly(ethylene oxide) (PEO, M_w = 900 000, Sigma-Aldrich), 3.8 mL of titanium isopropoxide (Ti(OiPr)$_4$, Sigma-Aldrich), 0.8 mL of acetic acid and 100 mL of ethanol. The precursor gel was then loaded into a plastic syringe and connected to a high-voltage power supply. The flow rate was 1.0 mL h^{-1} and the electric field strength was 0.8 kV cm^{-1}. The as-spun nanofibers were calcined at 450 °C for 1 h to remove organic components.

Fabrication of SDSCs based on mesoporous and regular NF photoelectrodes: In a standard fabrication process, the FTO glass (15 Ω/square, Asahi) was etched with Zn powder and HCl (4 M) to form the desired electrode pattern. The patterned substrates were ultrasonically cleaned with detergent, deionized water, acetone, and 2-propanol. A compact TiO$_2$ (c-TiO$_2$) film was then deposited onto FTO substrate by aerosol spray pyrolysis.[43] The paste used for device fabrication was made by mechanical grinding 0.1 g of mesoporous or regular NFs with 0.3 g of α-terpineol (98%, Acros) and 0.05 g of ethyl cellulose (Aldrich), which was then diluted with 2-methoxyethanol (1:1/ v:v). The NF paste was then spin-coated on the top of c-TiO$_2$ film to give a nanofibrous TiO$_2$ (nf-TiO$_2$) film. The thickness of the nf-TiO$_2$ film was controlled to be ~1.8 μm, by adjusting the spin-coating speed. Samples were then sintered at 450 °C for 30 min. After cooling, the films were soaked in TiCl$_4$ aqueous solution (40 mM) for 30 min at 70 °C. After rinsing with deionized water and ethanol, the films were sintered again at 450 °C for 15 min and sensitized with indoline dye D131 (0.3 mM in ethanol) for 12 hours at room temperature in the dark. The films were rinsed in ethanol and dried in N$_2$ flow. After that, the films were immersed into an acetonitrile solution containing Li(CF$_3$SO$_2$)$_2$N (Aldrich, 3 mg mL^{-1}) and 4-tert-butylpyridine (TBP, 60 mg mL^{-1}, Aldrich) for 2 min, and dried in air flow. Poly(3-hexylthiophene) (P3HT) (Rieke Met. Inc.) in chlorobenzene (15 mg mL^{-1}) was then spin-coated onto the dye-anchored TiO$_2$ films. The films were then transferred into the high vacuum chamber (3×10^{-4} Pa). Ag (60 nm in thickness) were subsequently deposited onto the P3HT layer as the back electrode. The device area was defined as the overlap between the FTO anode and back cathode (0.10 cm^2).

Characterization: Without sputtering gold, morphologies of mesoporous and regular NFs (as-spun and calcined) were characterized by a scanning electron microscope (SEM; Quanta 200 FEG System: FEI Company, USA) operated at 15 kV. The calcined TiO$_2$ nanofibers were further examined by transmission electron microscopy (TEM; JEM 2010F, JEOL, Japan) and selected area electron diffraction (SAED) operated at 200 kV with a drop of TiO$_2$ nanofiber suspension in methanol mounted onto a carbon-coated 200 mesh Cu grid. The crystal structure of TiO$_2$ nanofibers was investigated by an X-ray diffraction technique (XRD-6000, Shimadzu, Japan) using Ni-filtered Cu Kα line (λ = 0.15418 nm) at a scanning rate of 2° min^{-1} in 2θ ranging from 20° to 80°. The porous properties of the nf-TiO$_2$ films were characterized using N$_2$ adsorption at −196°C on a Multi-Station High Speed Gas Sorption Analyzer (Quantachrome, NOVA 3000). The samples (100 mg) were obtained by scratching the calcined nf-TiO$_2$ films from the FTO substrates. Prior to adsorption, the samples were degassed at 200°C overnight. The Brunauer–Emmett–Teller (BET) method was used to determine the specific surface area of the samples in the relative pressure range (P/P$_0$) of 0.05–0.35. The desorption data of the N$_2$ isotherm were analyzed by Barrett-Joyner-Halenda (BJH) method to give the total pore volume, pore size, and size distribution. Photocurrent measurements of the SDSCs were conducted under irradiation of a 100 mW cm^{-2} xenon lamp (Thermo Oriel Xenon Lamp 150W: Model 66902) with global AM1.5 condition. The intensity of incident light was calibrated using a reference cell (OptoPolymer, ISE CalLab) before each experiment. Photocurrent density–voltage curves of SDSCs were recorded by the electrochemical workstation (PGSTAT30, Autolab). Incident photon-to-current conversion efficiency (IPCE) was measured using a 300 W xenon light source (MAX-310, Asahi Spectra) and a monochromator (TMS300, Bentham). All the measurements were performed in air. The dye loading was determined by desorbing the dye in 0.36 M NaOH in methanol and measuring the UV-Vis absorption spectrum at 425 nm.[44] Intensity modulated photocurrent spectroscopy (IMPS) and intensity modulated photovoltage spectroscopy (IMVS) measurements were conducted using autolab electrochemical workstation equipped with a frequency response analyzer to drive a high-intensity blue LED (λ = 470 nm). The analysis of the photocurrent or photovoltage response of the cells was conducted in the frequency range of 10^4-1 Hz. The LED supplied the ac (modulation depth 10%) and dc components of the illumination. The light intensity was adjusted to be 12 mW cm^{-2} by neutral density filters (Schott NG) and measured by a calibrated silicon photodiode.[44]

Supporting Information

Supporting Information is available from the Wiley Online Library or from the author.

Acknowledgements

[1] U. Bach, D. Lupo, P. Comte, J. E. Moser, F. Weissörtel, J. Salbeck, H. Spreitzer, M. Grätzel, *Nature* **1998**, *395*, 583.

[2] S. Günes, N. S. Sariciftci, *Inorganica Chimica Acta* **2008**, *361*, 581.

[3] H. J. Snaith, A. J. Moule, C. Klein, K. Meerholz, R. H. Friend, M. Grätzel, *Nano lett.* **2007**, *7*, 3372.

[4] M. K. Nazeeruddin, F. De Angelis, S. Fantacci, A. Selloni, G. Viscardi, P. Liska, S. Ito, B. Takeru, M. Grätzel, *J. Am. Chem.Soc.* **2005**, *127*, 16835.

[5] L. Schmidt-Mende, S. M. Zakeeruddin, M. Grätzel, *Appl. Phys. Lett.* **2005**, *86*, 013504.

[6] M. L. Schmidt, U. Bach, B. R. Humphry, T. Horiuchi, H. Miura, S. Ito, S. Uchida, M. Grätzel, *Adv. Mater.* **2005**, *17*, 813.

[7] S. Kim, J. K. Lee, S. O. Kang, J. Ko, J.-H. Yum, S. Fantacci, F. De Angelis, D. Di Censo, M. K. Nazeeruddin, M. Grätzel, *J. Am. Chem. Soc.* **2006**, *128*, 16701.

[8] R. Zhu, C. Y. Jiang, B. Liu, S. Ramakrishna, *Adv. Mater.* **2009**, *21*, 994.

[9] M. Zukalová, A. Zukal, L. Kavan, M. K. Nazeeruddin, P. Liska, M. Grätzel, *Nano Lett.* **2005**, *5*, 1789.

[10] H. J. Snaith, M. Grätzel, *Adv. Mater.* **2007**, *19*, 3643.

[11] J. R. Jennings, L. M. Peter, *J. Phys. Chem. C* **2007**, *111*, 16100.

[12] K. Zhu, T. B. Vinzant, N. R. Neale, A. J. Frank, *Nano Lett.* **2007**, *7*, 3739.

[13] J. R. Jennings, A. Ghicov, L. M. Peter, P. Schmuki, A. B. Walker, *J. Am. Chem. Soc.* **2008**, *130*, 13364.

[14] S. H. Kang, S. H. Choi, M. S. Kang, J. Y. Kim, H. S. Kim, T. Hyeon, Y. E. Sung, *Adv. Mater.* **2008**, *20*, 54.

[15] B. Tan, Y. Wu, *J. Phys. Chem. B* **2006**, *110*, 15932.

[16] S. Pavasupree, S. Ngamsinlapasathian, M. Nakajima, Y. Suzuki, S. Yoshikawa, *J. Photochem. Photobiol. A: Chem.* **2006**, *184*, 163.

[17] G. K. Mor, K. Shankar, M. Paulose, O. K. Varghese, C. A. Grimes, *Appl. Phys. Lett.* **2007**, *91*, 152111.

[18] K. Shankar, G. K. Mor, H. E. Prakasam, O. K. Varghese, C. A. Grimes, *Langmuir* **2007**, *23*, 12445.

[19] S. Tepavcevic, S. B. Darling, N. M. Dimitrijevic, T. Rajh, S. J. Sibener, *Small* **2009**, *5*, 1776.

[20] K. M. Coakley, Y. Liu, M. D. McGehee, K. L. Frindell, G. D. Stucky, *Adv. Func. Mater.* **2003**, *13*, 301.

[21] G. K. Mor, S. Kim, M. Paulose, O. K. Varghese, K. Shankar, J. Basham, C. A. Grimes, *Nano Lett.* **2009**, *9*, 4250.

[22] C. J. Brinker, Y. Lu, A. Sellinger, H. Fan, *Adv. Mater.* **1999**, *11*, 579.

[23] D. Li, Y. Xia, *Nano Lett.* **2003**, *3*, 555.

[24] D. Li, J. T. McCann, Y. Xia, *J. Am. Ceram. Soc.* **2006**, *89*, 1861.

[25] A. Kumar, R. Jose, K. Fujihara, J. Wang, S. Ramakrishna, *Chem. Mater.* **2007**, *19*, 6536.

[26] K. Fujihara, A. Kumar, R. Jose, S. Ramakrishna, S. Uchida, *Nanotechnology* **2007**, *18*, 365709.

[27] R. Zhu, C. Y. Jiang, X. Z. Liu, B. Liu, A. Kumar, S. Ramakrishna, *Appl. Phys. Lett.* **2008**, *93*, 013102.

[28] Y. D. Wang, C. L. Ma, X. D. Sun, H. D. Li, *Mater. Lett.* **2002**, *54*, 359.

[29] P. Scherrer, *Göttinger Nachrichten* **1918**, *2*, 98.

[30] P. Yang, D. Zhao, D. I. Margolese, B. F. Chmelka, G. D. Stucky, *Chem. Mater.* **1999**, *11*, 2813.

[31] Y. Yue, Z. Gao, *Chem. Comm.* **2000**, 1755.

[32] M. Wei, Y. Konishi, H. Zhou, M. Yanagida, H. Sugihara, H. Arakawa, *J. Mater. Chem.* **2006**, *16*, 1287.

[33] J. van de Lagemaat, K. D. Benkstein, A. J. Frank, *J. Phys. Chem. B* **2001**, *105*, 12433.

[34] M. Grätzel, *Acc. Chem. Res.* **2009**, *42*, 1788.

[35] J. Krüger, R. Plass, M. Grätzel, P. J. Cameron, L. M. Peter, *J. Phys. Chem. B* **2003**, *107*, 7536.

[36] J. van de Lagemaat, A. J. Frank, *J. Phys. Chem. B* **2001**, *105*, 11194.

[37] K. D. Benkstein, N. Kopidakis, J. van de Lagemaat, A. J. Frank, *J. Phys. Chem. B* **2003**, *107*, 7759.

[38] M. J. Cass, A. B. Walker, D. Martinez, L. M. Peter, *J. Phys. Chem. B* **2005**, *109*, 5100.

[39] B. H. Lee, M. Y. Song, S.-Y. Jang, S. M. Jo, S.-Y. Kwak, D. Y. Kim, *J. Phys. Chem. C* **2009**, *113*, 21453.

[40] G. Schlichthörl, N.-G. Park, A. J. Frank, *J. Phys. Chem. B* **1999**, *103*, 782.

[41] M. Wang, S. J. Moon, M. Xu, K. Chittibabu, P. Wang, N. L. Cevey-Ha, R. Humphry-Baker, S. M. Zakeeruddin, M. Grätzel, *Small* **2010**, *6*, 319.

[42] J. M. Zhuo, L. H. Zhao, R. Q. Png, L. Y. Wong, P. J. Chia, J. C. Tang, S. Sivaramakrishnan, M. Zhou, E. C. W. Ou, S. J. Chua, W. S. Sim, L. L. Chua, P. K. H. Ho, *Adv. Mater.* **2009**, *21*, 4747.

[43] L. Kavan, M. Grätzel, *Electrochim. Acta* **1995**, *40*, 643.

[44] W. H. Howie, F. Claeyssens, H. Miura, L. M. Peter, *J. Am. Chem. Soc.* **2008**, *130*, 1367.